# Aerosol Jet Printed Organic Memristive Microdevices Based on a Chitosan:PANI Composite Conductive Channel

Roman Sajapin, Davide Vurro, Pasquale D'Angelo,* Giuseppe Tarabella, Simone L. Marasso, Matteo Cocuzza, Maddalena Botti, Mirko Buttrini, Adriana Calderaro, Tatiana Berzina, and Salvatore Iannotta*

Read Online

ACCESS | Metrics & More | Article Recommendations

**ABSTRACT:** In this study we show a chitosan:polyaniline (CPA)-based ink, responding to eco-biofriendly criteria, specifically developed for the manufacturing of the first organic memristive device (OMD) with an aerosol jet printed conductive channel. Our contribution is in the context of bioelectronics, where there is an increasing interest in emulating neuromorphic functions. In this framework, memristive devices and systems have been shown to be well suited. In particular organic-based devices are envisaged as very promising in some applications, such as brain−machine interfacing, owing to specific properties of organics (e.g., biocompatibility, mixed ionic−electronic conduction). On the other hand, the research activities on flexible organic (bio)electronic devices and direct writing (DW) noncontact techniques increasingly overlap in the effort of achieving reliable applications benefiting from the rapid prototyping to accomplish a fast device optimization. In this context, ink-based techniques, such as aerosol jet printing (AJP), although particularly well suited to implement 3D-printed electronics due to advantages it offers in terms of a wide set of allowed printable materials, still require research efforts aimed at conferring printability to the desired precursors. The developed CPA composite was characterized by FTIR, DLS, and MALDI-TOF techniques, while the related aerosol jet printed films were studied by SEM and profilometry. Taking advantage of the intrinsic and stable electrical conductivity of CPA films, which do not necessarily require any acidic treatment to promote a sustained charge carrier conduction, 10 $\mu$m short-channel OMDs were hence manufactured by interfacing the printed CPA layers with a solid polyelectrolyte (SPE). We accordingly demonstrated prototypes of stable and best performing OMD devices with downscaled features, showing well-defined counterclockwise hysteresis/rectification and an enhanced durability. These properties pave the way to further improving performance, as well as to realizing a direct integration of the devices into hardware neural networks by in-line fabrication routes.

**KEYWORDS:** *aerosol jet printing, PANI, organic memristor, green printing ink, solid polyelectrolyte*
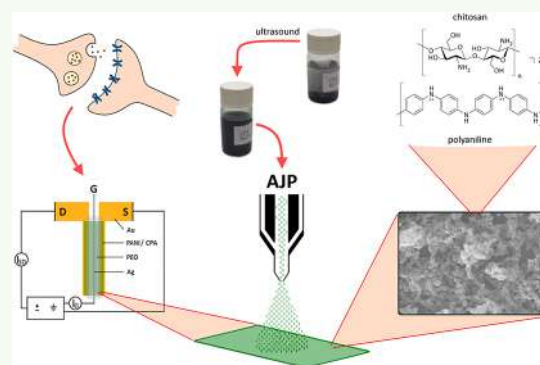
## 1. INTRODUCTION

Memristive devices and systems represent a still emerging but fast-growing field for information technologies, with envisioned applications in memories, neuromorphic computing systems, artificial neural networks (ANNs), and computer−brain interfaces.[1−5] The hardware realization of novel neuromorphic computing systems is fostered by memristors considering that their electrical response well mimics a biological synapse. More specifically, the dependence of the memristor's conductive state on the charge carriers flowing in its active channel, i.e., its history of use, corresponds to the typical spike-timing-dependent plasticity (STDP) of synapses, well known in neurosciences.[6] The analogy to biological nervous systems is at the basis of the development of computational systems where memristive elements simultaneously play a key role in both the storage and the processing of information, hence going beyond the typical Von Neumann architecture in which the information is constantly exchanged between the processor and the memory.

Most of the available memristive devices are based on inorganic materials such as metal/metal oxides (TiO$_2$, HfO$_x$, NiO, CuO, SiO$_2$, and many others[7]). Their operation relies on the formation and disruption of conductive filament structures. These devices are characterized by an abrupt switching

behavior, making them particularly suitable for memories and binary data processing. Although less extensive, research efforts have also been devoted to investigating devices based on organic materials. Their expected main advantages are cost efficiency, superior processability, flexibility, and other peculiar mechanical properties.[8,9] One of the first and best-studied organic-based memristors is the so-called organic memristive device (OMD).[10] The OMD is a three-terminal device based on polyaniline (PANI), a redox-active material acting as the conductive OMD channel defined between two metal electrodes, i.e., the grounded source and the biased drain terminals. The active channel is interfaced with a polyelectrolyte (in our setup a poly(ethylene oxide) (PEO)-based solid polyelectrolyte, SPE) in which a third controlling terminal (i.e., the gate) made of a grounded silver electrode is immersed. This architecture favors the conductivity switch of PANI from nonconductive leucoemeraldine (LE) to the conductive emeraldine salt (ES) form, due to redox processes involving the PANI film and ionic species of the electrolyte.[11,12] The silver electrode functions as a redox reaction partner for PANI, being transformed from Ag to AgCl and vice versa when PANI is reduced and oxidized, respectively. A counterclockwise hysteresis in current−voltage ($I-V$) measurements is observed upon cyclically varying the channel voltage in a low-voltage window ($< \pm 1$ V).[10] Various distinct conductive states can be established due to the gradual switching of PANI. The memristive hysteresis may therefore be ascribed to the different kinetics between the anodic and cathodic redox processes.

OMDs arouse particular interest because they are promising candidates to be implemented in computer−brain interfaces, being well-suited to emulate the synaptic behavior, including short-term and long-term plasticity.[13] Such devices have been successfully tested in a fully hardware perceptron-like neural network.[14] However, so far major manufacturing steps of the prototypes, such as the deposition of the conductive PANI channel or the deposition of the solid polyelectrolyte, have been carried out manually on a rather macroscopic (millimeter) scale. Currently, there have been severe limitations in reproducibility of the device response and in switching time, which is quite high and typically larger than 100 s. Progress has been made recently by Lapkin et al.[15] and Battistoni et al.,[16] who made first improvements toward the miniaturization by manufacturing 20−200 $\mu$m long channels and using a PEO-based SPE or a liquid electrolyte (aqueous HCl), respectively. A significant enhancement of the switching rates has been demonstrated in these works. However, in both papers, the active channels were made by depositing PANI by means of the quite time-consuming Langmuir−Schaefer (LS) technique.

In the framework of miniaturization, the implementation of automated manufacturing for this type of devices is strongly needed but has not yet been available. Besides the potential minimization of device-to-device variability, the main advantages of automated manufacturing are the large timesaving and the very low waste achievable by maskless patterning processes. This is also well suited for high-resolution, rapid prototyping manufacturing of large-area, flexible electronic devices.[17]

Direct writing (DW) noncontact techniques have emerged as a new paradigm for mesoscale electronics, since the Defense Advanced Research Projects Agency (DARPA) introduced the Mesoscopic Integrated Conformal Electronics (MICE) Program (2002).[18] Currently, the available DW processes (i.e.,

inkjet printing, IJP, and aerosol jet printing, AJP) are promising for a further downscaling of device features, being a prerequisite for mass production, faster kinetics, and higher performance. IJP and AJP allow the printing of materials starting from the solution of a dedicated ink formulation, but in the case of AJP the ink is nebulized by means of a pneumatic or an ultrasonic atomizer, forming an aerosol. The droplets are hence ejected from an orifice (the nozzle) and impact on a substrate placed on a moving plate, replicating the CAD layout pattern. AJP exploits the combined action of two gas flows, one acting on the transport of aerosolized inks toward the nozzle (carrier gas flow, CGF) and the other forcing the generated aerosol along the central axis of the stream, confining and collimating it (sheath gas flow, ShGF). Accordingly, compared to IJP, this technique allows both a higher resolution (narrow line width below 10 $\mu$m[19]) and ensures printability of higher viscosity inks (ink viscosity ranging between 1 and 1000 cP[20,21]). Although AJP is more recent and hence less mature than IJP, it is particularly well suited for 3D-printed flexible electronics.[17,22−24]

Some earlier works have been devoted to DW approaches where PANI was doped by sulfonic acid or was a nanofibrous material for applications in sensor technology.[25−28] Here, we report on the development of two different novel types of PANI-based inks, well suited for AJP systems. The produced materials have been first characterized by SEM and current−voltage measurements to explore the formation and optimization of well-defined, compact, and conducting films by the developed inks. Our optimal formulation turned out to be a water/isopropyl alcohol (IPA)-based suspension of a chitosan/PANI composite (CPA), which has been used to fabricate the first organic memristive microdevice manufactured by using the AJP technique for depositing a PANI conductive layer acting as the OMD active channel. The device performance is based on the interface between the as-deposited CPA and an $AlCl_3$-doped PEO-based SPE. The device response shows the typical well-defined OMD behavior, with a proper hysteresis/rectification of current−voltage curves, which remain practically unchanged over a series of cyclic measurements.

## 2. MATERIALS AND METHODS

**2.1. Preparation of PANI-Based Inks.** For the pure PANI-based ink, we used a nearly saturated 1.0 mg/mL solution of polyaniline (Sigma-Aldrich, $M_w$ = 105 Da) in an opportune mixture of solvents made of NMP/xylene/IPA (1:1:2 $v/v/v$). Solvents, all classified as ACS grade, were purchased from Sigma-Aldrich. PANI was first slowly added to $N$-methyl-2-pyrrolidone (NMP) under stirring until the dissolution of aggregates, followed by slow dilution with toluene and then IPA. The ink was vigorously stirred for 30 min at room temperature before use.

The second, improved CPA-based ink was made as a 2.0 mg/mL suspension in $H_2O$/IPA (4:1 $v/v$). It was synthesized from aniline in the presence of predissolved, low molecular weight chitosan, following an oxidative polymerization mechanism and using ammonium persulfate (APS) as the oxidizing agent, based on the protocol suggested by Ratuchne et al.[29] First, 0.3 g of chitosan (Sigma-Aldrich) was dissolved in 50 mL of 4 % acetic acid (VWR Chemicals), and the solution was cooled in an ice bath. Separately, 0.9313 g (10 mmol) of aniline (Merck) was dissolved in 50 mL of 1 M hydrochloric acid (Carlo Erba) and added dropwise to the chitosan solution under stirring. A few drops of a 1 M $FeSO_4$ (VWR Chemicals) solution were added to the mixture. Lastly, a cooled solution of 2.7382 g (12 mmol) of APS (Acros Organics) in 40 mL of 1 M hydrochloric acid was added dropwise to the reaction mixture over ca. 1 h under vigorous
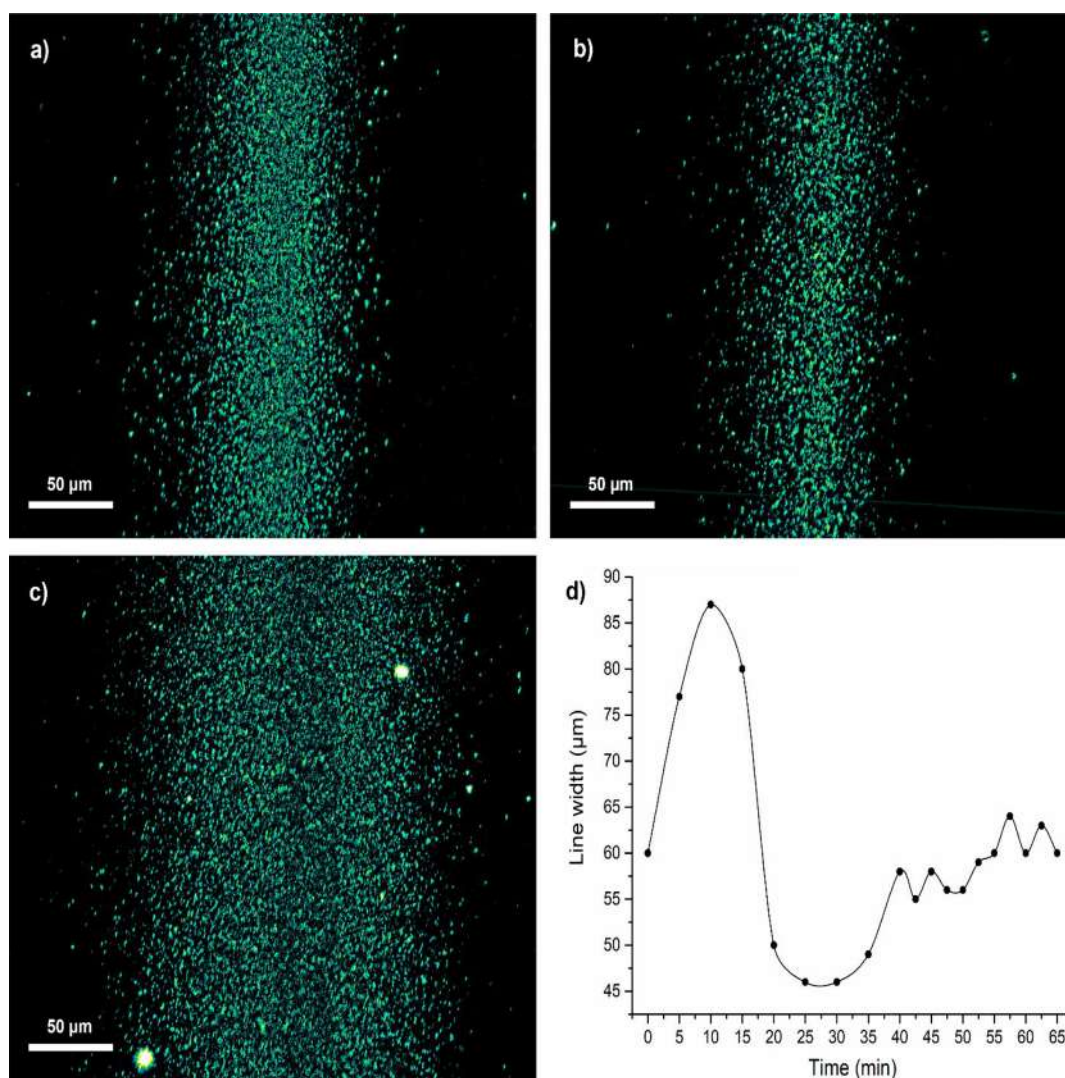
**Figure 1.** Printed line features with different printing parameters: (a) ShGF = 40 sscm, CGF = 30 sscm (FR = 1.33), sample stage speed = 0.5 mm/ s (as used for channel depositions); (b) ShGF = 40 sscm, CGF = 30 sscm (FR = 1.33), stage speed = 2.0 mm/s; (c) ShGF = 35 sscm, CGF = 23 sscm (FR = 1.52), stage speed = 0.5 mm/s. (d) Characterization of the printing process drift and the stabilization of the line features. During the first 20 min of the stabilization process, the ink line is dominated by an excessive amount of solvent while little material is atomized. This leads to a broadening of the line and ill-defined features with pronounced edges but an empty core. Upon stabilization of the gas fluxes as well as an increasing atomization of the material, a more homogeneous line definition is achieved, and the width reaches a plateau with minor fluctuations after ca. 40 min.

stirring, maintaining the temperature below 5 °C. The mixture was then stirred for 12 h, and its color changed from pale yellow to bluish-green to dark green. The excess APS was quenched by adding 5 mL of a 1 M $FeSO_4$ solution. The resulting suspension was centrifuged at 4000 rpm for 5 min. The light green supernatant was discarded, and the dark green solid product was resuspended in 1 M hydrochloric acid and centrifuged. The last step was repeated three times. The pellet was then resuspended once more in acetone, centrifuged, and dried at 50 °C for 24 h. Lastly, the dark green, brittle solid product was ground in an agate mortar.

**2.2. Materials Characterizations.** FTIR spectroscopy has been used to first characterize the CPA compound features. The analysis has been carried out on a PerkinElmer Spectrum Two, preparing the sample as a KBr pellet.

Differential light scattering (DLS) analysis has been used to characterize the characteristic size of CPA particulates on a Zeta Plus with a 635 nm, 15 mW laser source in the transmission mode. The measurement was carried out on a 0.1 mg/mL suspension in water in a PMMA cuvette. Prior to the analysis, the sample was treated with

ultrasound for 5 min using an Elma Elmasonic P ultrasonic bath ($P$ = 120 W, $f$ = 37 kHz) to avoid the formation of aggregates.

MALDI-TOF mass spectrometry has been used to provide further insight into the molecular weight of the synthesized CPA composite. The measurements were carried out on a Bruker Syrius spectrometer, using $\alpha$-cyano-4-hydroxycinnamic acid (HCCA) as the matrix material solubilized in organic solvent OS-TA30 (30:70 acetonitrile (ACN)/0.01 % trifluoroacetic acid). The spectra were acquired in the positive linear mode in the range of 2−20 kDa with a 60 Hz laser frequency and an ion source voltage of 20 kV. The acquired spectra were analyzed with FlexAnalysis software (v.3.1, Bruker), normalized by "smoothing" and "baseline" functions.

SEM analysis has been carried out on printed layers of pure PANI (4 AJP layers, 30 K magnification) and CPA-based (1 AJP layer, 20 K magnification) using a SEM-FIB Zeiss Auriga Compact (ETH 15 kV) in order to determine the quality of printed PANI-based films.

Profilometry measurements were performed on a Bruker Dektat XT profilometer. AFM micrographs have been acquired in tapping mode, using a Dimension 3100 scanning probe microscope equipped with a Nanoscope IV controller (Veeco Instruments) with the aim of
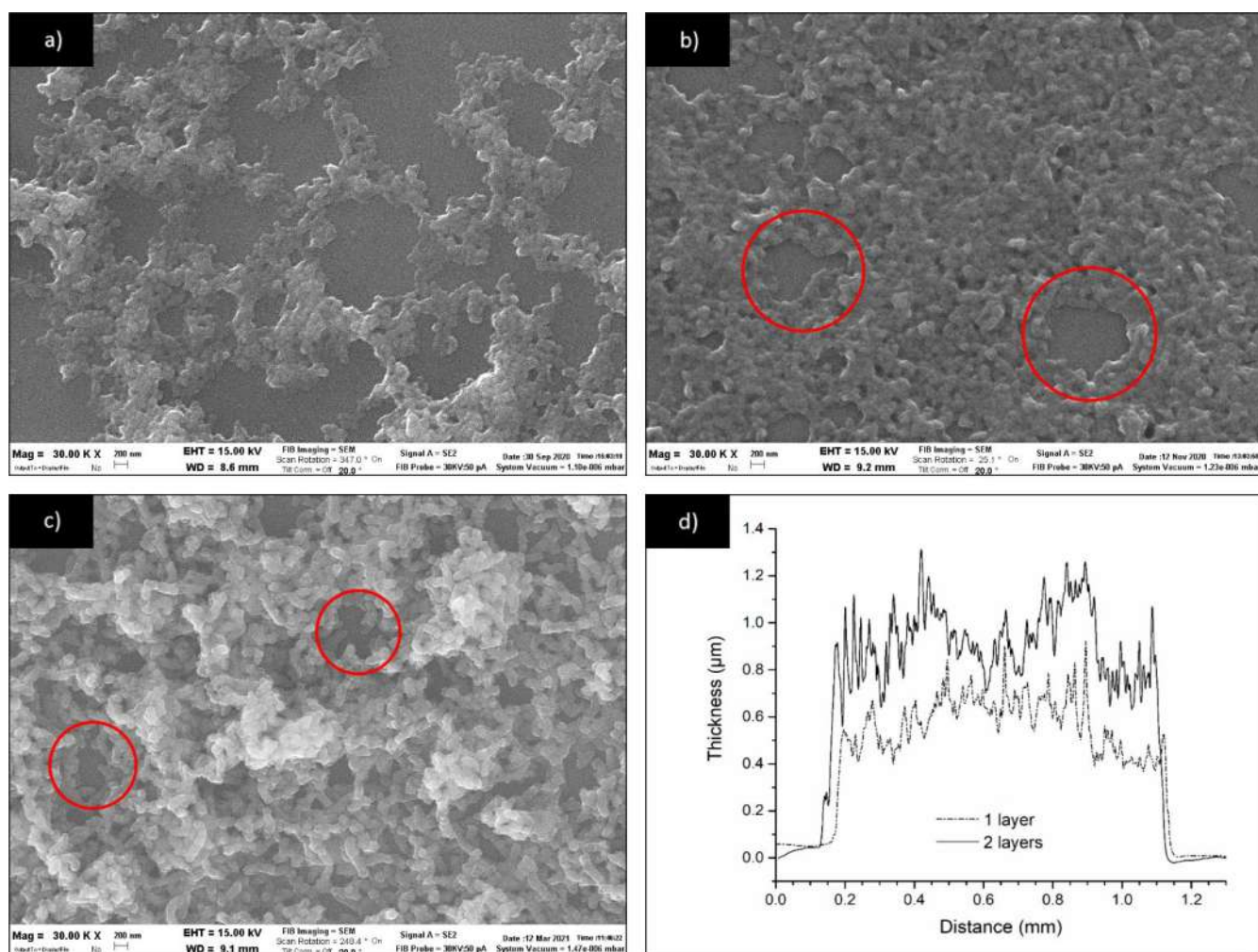
**Figure 2.** SEM images of AJP printed films of (a) pure PANI-EB (10 layers) without surface pretreatment, (b) pure PANI-EB (4 layers) after $O_2$/Ar plasma treatment, and (c) CPA (single layer) on a Si/SiO$_2$ substrate with pinholes highlighted in red. (d) Thickness profile of printed films consisting of one and two layers (different samples), acquired from profilometry measurements.

estimating the thickness of the as-deposited films. The measurements were acquired near the edge of the deposited layer.

**2.3. Ink Deposition with AJP.** Pure PANI-EB- and CPA-based inks have been deposited on a Si/SiO$_2$ (1 $\mu$m of thermal oxide layer) substrate with T-shaped gold source and drain electrodes ($d_{SD}$ = 10 and 200 $\mu$m for pure PANI and 10 $\mu$m for CPA, channel width fixed at $W$ = 4 mm), prefabricated by photolithography, already reported elsewhere.[30] The deposition of the inks has been carried out with an Optomec AJP 200 system, using an ultrasonic atomizer and the following deposition parameters: nozzle diameter $d$ = 200 $\mu$m; ShGF = 40 sccm; CGF = 30 sccm; deposition stage speed = 0.5 mm/s; stage temperature = 90 °C, both for pure PANI-EB- and CPA-based inks. Substrate surface treatment by UV-ozone cleaning with a PSD series UV cleaner (Novascan) was used to improve the surface wettability and, accordingly, decreasing the necessary number of deposited layers. A preliminary characterization of the line features depending on the printing parameters is shown in Figure 1a−c, demonstrating a deposition in a spray-like regime. The ink was atomized and jetted for 1 h as a stabilization check before the printing session. As it is shown in Figure 1d, the line width varies significantly during the first 40 min of deposition, after which only minor fluctuations occur.

**2.4. OMD Fabrication and Characterization of the Related Electrical Response.** OMD devices have been completed by interfacing the PANI channels (two printed layers, thickness estimated by AFM around 2 $\mu$m) connecting the T-shaped source and drain electrodes with an SPE based on PEO ($M_w$ = 8 MDa, Sigma-Aldrich) doped with AlCl$_3$ (Acros Organics). The SPE was prepared by adding PEO to an aqueous solution of AlCl$_3$ (0.1 mol/L) and LiClO$_4$ (0.05 mol/L) and letting it swell to homogeneity over 2 days. The PEO was drop cast as a gel and allowed to solidify at room temperature after immersing a silver wire ($d$ = 50 $\mu$m) as the gate electrode perpendicular to the printed channel area. To prevent a short circuit between the gate and the channel, the silver wire was placed on spacers made from strips of polyimide tape (Kapton).

The characterization of the memristive properties by the printed devices has been carried out by acquiring the channel current ($I_{EL}$) as a function of the channel voltage ($V_{SD}$). The latter parameter was cyclically swept between −0.4 and +0.6 V in the forward and backward scan mode at different scan rates (10−100 mV/s) with a step of 0.02 V. Measurements have been carried out by using a two-channel source-meter precision unit (Agilent B2902A) driven by the open source Quick-IV Measurements software.

## 3. RESULTS AND DISCUSSION

**3.1. Pure PANI-Based Inks for AJP.** The major difficulty in printing PANI by DW noncontact techniques is due to its poor solution processability, since pure PANI ($M_w$ = 100 kDa), commonly used in OMD manufacturing, dissolves reliably only in NMP, which is hazardous and disadvantageous for use in AJP due to its low volatility. Hence, our first approach was to respond to the requirements of solvent compatibility with the AJP system. We prepared a printable PANI suspension in a
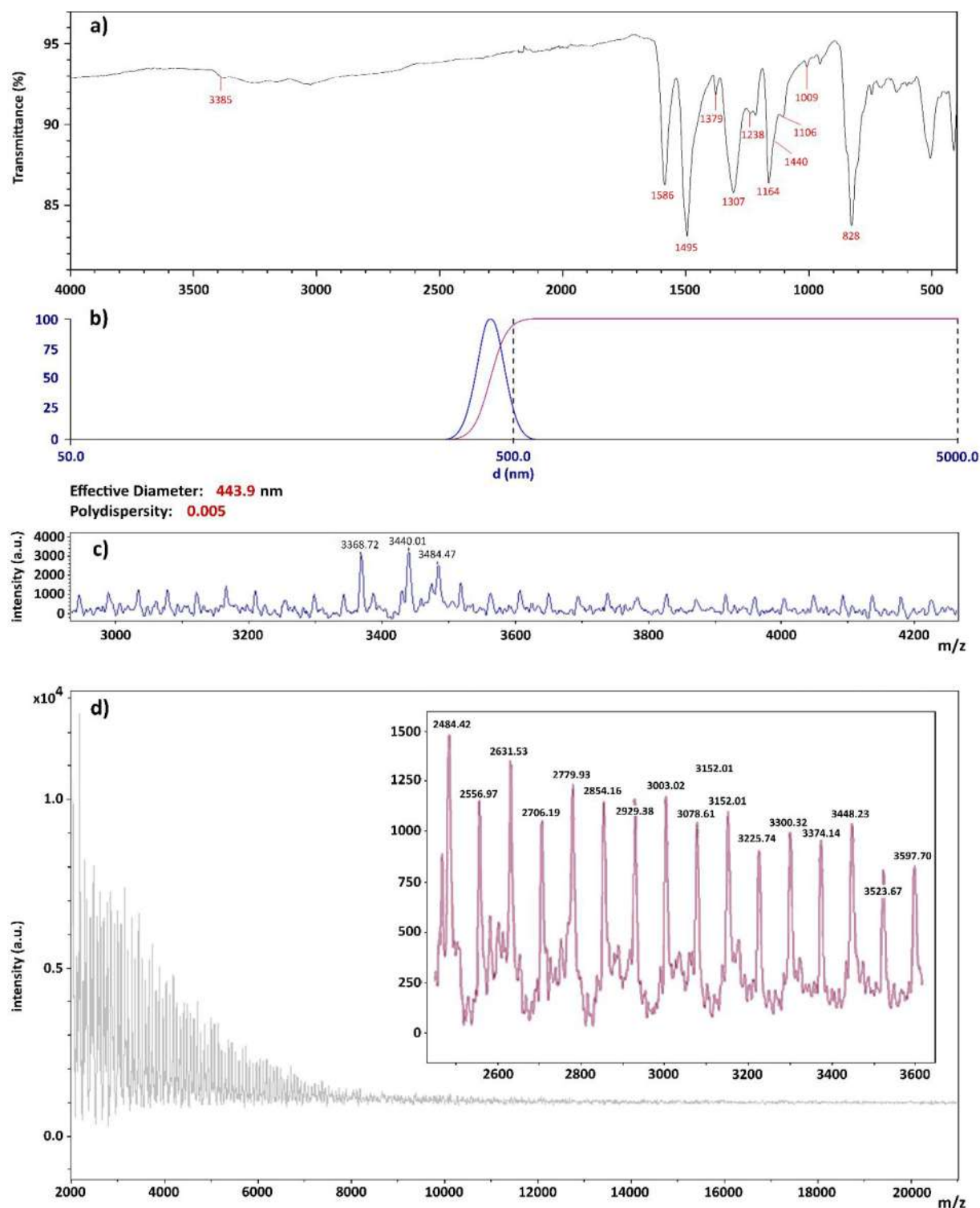
**Figure 3.** (a) FTIR spectrum of the synthesized CPA composite (KBr pellet). (b) DLS analysis of a 0.1 mg/mL CPA suspension in water. The sample was sonicated for 5 min prior to the measurement. (c) MALDI-TOF mass spectra of the synthesized CPA composite deposited on the substrate as a dispersion in $H_2O$/ACN (1:1 $v/v$) and (d) as a solution in $H_2O$/HFIP (1:1 $v/v$). The baselines are subtracted, and the margin of error is 1000 ppm.

solvent mixture of NMP, xylene, and IPA (2.1. Preparation of PANI-Based Inks), aiming at improving the volatility of the ink, hence enabling its deposition and avoiding PANI precipitation. Such solvent formulation allows to minimize the overspray phenomenon[31] and is expected to reduce the known nozzle clogging issues. We hence deposited 10 layers of

this ink onto a Si/SiO$_2$ substrate, as described in the experimental section (2.3. Pure PANI and CPA-Based Ink Deposition by AJP). The poor quality of the resulting deposited features, characterized by a large porosity and poor connectivity (Figure 2a), has been improved in successive deposition runs by increasing the wettability of the substrate
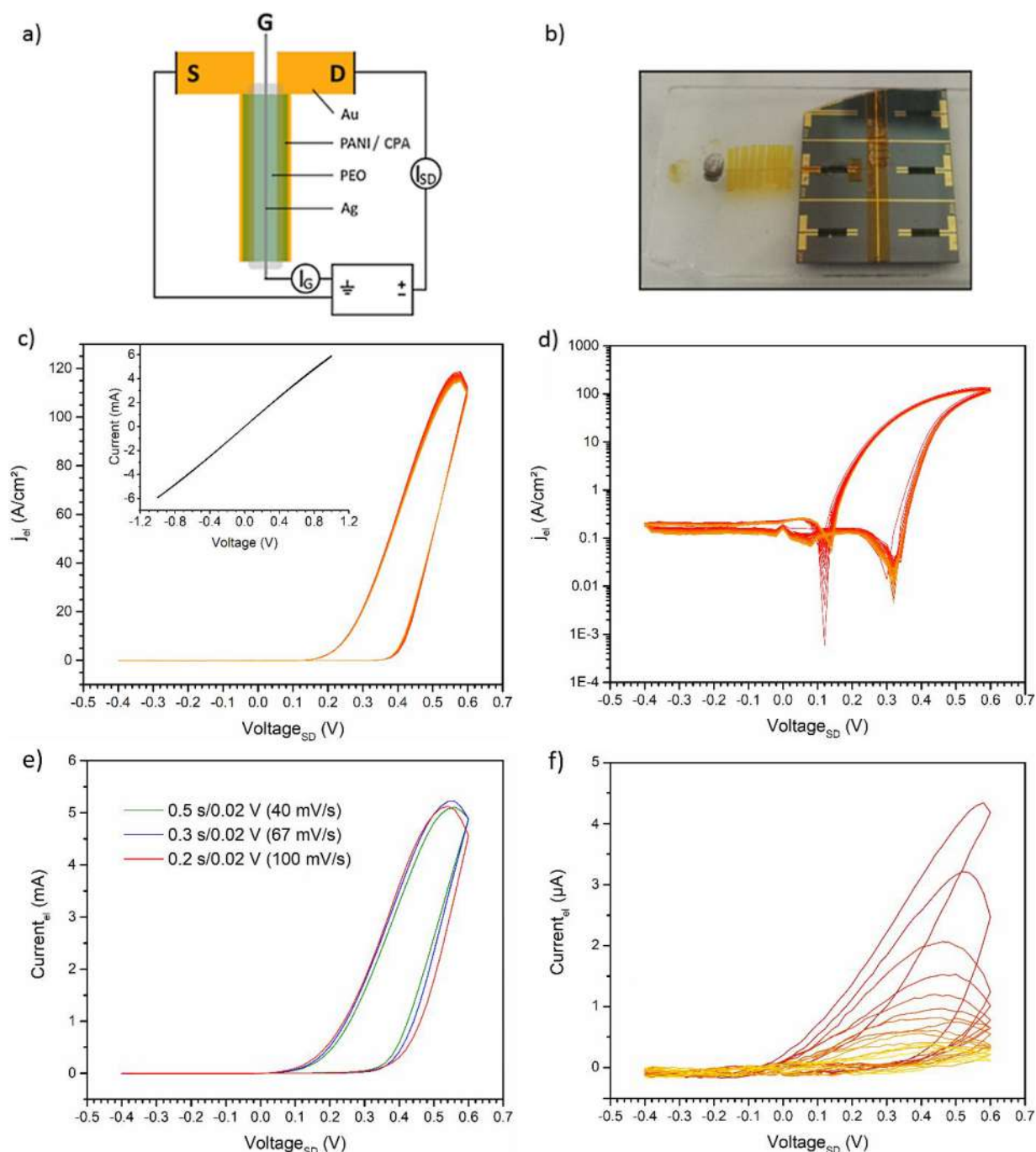
**Figure 4.** (a) Schematic representation of the memristive microdevice with an AJP printed conductive layer. (b) Example of a fabricated OMD with a printed CPA layer. (c, d) 40 consecutive $I-V$ cycles measured at a scan rate of 10 mV/s on an OMD fabricated with two printed CPA layers as the conductive channel and an $AlCl_3$-doped, PEO-based SPE on a $Si/SiO_2$ substrate with Au electrodes and $d_{SD}$ = 10 $\mu$m. The conductivity changes from $7.53 \times 10^{-3}$ to 0.22 S/cm upon transitioning between the off- and on-state. In the inset in (c), the almost ideal ohmic behavior by the as-deposited CPA layer is demonstrated. (e) $I-V$ characterization of the device at higher scan rates. (f) Reference measurement of a standard OMD fabricated with pure PANI deposited by LS (15 cycles).

through pretreating the sample surface with UV-ozone (50 °C, 3 min) and $O_2$/Ar plasma (3 W, 9 min) cleaning procedures, hence decreasing the necessary number of printed layers to 4. Despite the relevant improvement, the coverage remains somewhat nonuniform and the layers include relatively large pinholes ($d \approx 0.5$ $\mu$m, as shown in the SEM image reported in Figure 2b). This is due to both the poor solubility of PANI in the solvent mixture and the low volatility of NMP. From the point of view of the electrical properties the printed layers

displayed the following resistances: 6500 $\Omega$ ($\rho$ = 20 $\Omega$ cm) for a film with $d_{SD}$ = 200 $\mu$m, which could be decreased to 340 $\Omega$ ($\rho$ = 1.1 $\Omega$ cm) upon PANI protonation by a treatment with 1 M aqueous HCl;[32] 500 $\Omega$ ($\rho$ = 32 $\Omega$ cm) for a film with $d_{SD}$ = 10 $\mu$m, decreased to 30 $\Omega$ ($\rho$ = 1.9 $\Omega$ cm) after treatment with HCl. Even though such results are quite interesting, they are not yet satisfactory considering the scale, thickness, and geometry of the channel, due to the ill-defined morphology as the main cause of the relatively low resulting conductivities.

**3.2. CPA-Based Inks for AJP.** To optimize the process and improve device performance, we then proceeded by developing a novel ink based on a chitosan/PANI composite, that we expected to be better suitable for AJP, as it does not require any high-boiling and/or toxic solvents such as NMP and xylene. The synthesis of CPA is described in the experimental section (see 2.1. PANI-Based Ink Preparation) and was inspired by a work by Ratuchne et al.[29] The material reported in that study is a soluble hybrid composite, produced by polymerization of aniline in the presence of chitosan in a hydrochloride acid medium. Conversely, our product, despite being insoluble in water, forms well-processable inks in the form of stable suspensions in $H_2O$/IPA (4:1 $v/v$). The presence of polyaniline in the conductive form, the green emeraldine salt, was confirmed by Fourier transform infrared spectroscopy (FTIR, reported in Figure 3a), featuring the characteristic absorption bands of this PANI state.[33] In particular, the following signals have been ascribed to the CPA composite:[34] $\delta_{op}(C-H)$ and $\delta_{ip}(C-H)$ in 1,4-disubstituted rings at 828 $cm^{-1}$ and 1106−1164 $cm^{-1}$; bipolaron $\nu(=NH^+-)$ at 1140 $cm^{-1}$ (shoulder band); polaron $\nu(C-N^{\bullet+})$ band at 1238 $cm^{-1}$; $\nu(C-N)$ of secondary aromatic amines at 1307 $cm^{-1}$; $\nu(C=N)$ in the vicinity of quinoid rings at 1379 $cm^{-1}$; benzenoid $\nu(C=C)$ at 1495 $cm^{-1}$; quinoid $\nu(C=C)$ at 1586 $cm^{-1}$; the absence of a sharp band around 3610−3645 $cm^{-1}$ indicates that no free chitosan −OH groups are present, suggesting that they participate in intermolecular hydrogen bonds, characterized by a broad band around 3200−3400 $cm^{-1}$; the broad band around 3000−3200 $cm^{-1}$ can be attributed to H-bound NH groups; the band at 3385 $cm^{-1}$ corresponds to free NH groups not participating in H-bonding; the small band at 1009 $cm^{-1}$ corresponds to $\nu(C-O)$ of the secondary cyclic alcohol moieties in chitosan.

A DLS study, performed on a suspension of the as-prepared product in deionized water, displayed a very narrow particle size distribution, with a mean hydrodynamic diameter of ca. 440 nm and a polydispersity of 0.005 (Figure 3b). The formation of clusters was avoided by treating the suspension in ultrasound for 5 min. It appears that the synthesis conditions provide a substantial control over the polymer chain length and the dimension of the resulting microparticles. This is most likely due to the poor solubility of the chitosan/PANI composite (or PANI in general) in water, causing the polymer chains to collapse and form coil-like structures when reaching a critical length. After this, larger particles do not form because of the preferential growth of shorter, still solvated chains.

Additional structural information was gained from MALDI-TOF mass spectrometry. The analysis has proven to be difficult because of the composite's solubility issues. The obtained dispersions in water, ACN, and 1,1,1,3,3,3,-hexafluoro-2-propanol (HFIP) adhered weakly on the substrate/matrix, often making an effective ionization difficult. As exemplified in Figure 3c, a group of signals around 3400 Da reoccurred in most of the acquired spectra. It appears that this formation is especially abundant and/or stable under the ionization conditions. The $m/z$ differences of the individual peaks are ca. 71.3 Da between the second and the first and ca. 115.8 Da between the third and the first one. These atomic weights likely correspond to a doping of imine nitrogen atoms by two HCl units (ca. 72.9 Da) or two $CH_3COOH$ units (ca. 120.1 Da), which are related to solvent traces remaining from the synthesis. The periodically occurring, weak signals in Figure 3c also differ by ca. 72 Da, further indicating the

presence of PANI chains with various levels of HCl doping. Similar results can be seen in Figure 3d, exhibiting the same periodicity of signals (see inset). The reoccurring signals around 3400 Da appear consistent with the narrow particle size distribution shown by DLS. However, the MALDI-TOF results do not allow a precise determination of the polymer chain length due to the possible copresence of chitosan and PANI chains with variable levels of doping, as well as aggregates that can form during the sample preparation.

Additional HCl doping of the chitosan/PANI layer after its deposition was not necessarily required for the functionality of devices as it was the case with layers made of pure PANI.[35] Furthermore, the use of inexpensive solvents (such as $H_2O$ and IPA), avoiding toxic ones (such as NMP and xylene), and the generally low-waste operation of the AJP make this approach a step toward an ecological friendliness of the manufacturing process.

The lower solubility of our material in comparison with the one synthesized by Ratuchne et al.[29] is apparently associated with a lower content of chitosan in our composite, which is consistent with the low intensity of signals associated with chitosan in the FTIR spectrum. The as-prepared suspension has then been deposited using the same printing parameters of the pure PANI-based ink in NMP/xylene/IPA discussed previously. A major result is that the favorable choice of solvents significantly improved the coverage of the $Si/SiO_2$ substrate by the CPA ink with respect to the one based on pure PANI, reducing both the amount and the average size of pinholes, as shown in the reported SEM image (Figure 2c). The average thickness of the CPA layer was estimated by profilometry, scanning across the whole width of the printed channel. Thicknesses of around 400−700 nm were acquired for single layers and around 800−1200 nm for two stacked layers due to tighter packing of the material (Figure 2d). These measurements confirmed the overall rough profile observed by SEM were validated by AFM, measured in a size window including the film edge.

OMDs featuring CPA channels (two printed AJP layers) were fabricated according to the scheme in Figure 4a). A silver wire, acting as the (silent) gate electrode, was immersed in a manually cast, $AlCl_3$-doped, PEO-based solid polyelectrolyte, interfaced with the CPA channel. The above SPE is a modified, more durable formulation of the standard $LiClO_4$-doped PEO, which significantly prolongs the durability of the polyelectrolyte due to a long-lasting retention of both its hydration state and necessary level of acidity. This formulation, together with other ones, is currently the subject of an optimization study that will be discussed in detail in a future upcoming work.

The $I-V$ characteristics of such a device, reported in Figure 4c, show the expected OMD switching onset at around +0.4 V, with a well-defined counterclockwise hysteresis curve and rectification at around +0.1 V. The voltage range was set between −0.4 and +0.6 V to avoid the second oxidation step of the conductive PANI-ES toward the nonconductive pernigraniline state, occurring at higher voltages during the anodic scan. Conversely, a complete reduction of the material is ensured during the cathodic scan. The device exhibits a good response reproducibility over 40 cycles with minimal output fluctuations. This is a major improvement with respect to standard OMDs characterized by a typical life span of ≤50 cycles and quite poor reproducibility, as demonstrated in Figure 4f. The operation scan rate was 10 mV/s, which could be easily

increased over 40 mV/s, as shown in Figure 4d. Further increase of the scan rate is limited by the switching kinetics, as the hysteresis begins to widen at higher scan rates of 67 and 100 mV/s. Considering the dimensions of the CPA channel with a width $W$ of 4 mm, a length $d_{SD}$ of 10 $\mu$m, and a mean film thickness of about 0.9 $\mu$m, as well as measured electrical resistance values $R$ as low as 14 $\Omega$ ($\rho$ = 0.50 $\Omega$ cm), the conductivity of our best obtained film is estimated to be about 2 S/cm, as opposed to typical values of about 50 S/cm for LS films. In an array of nine different printed channels, a mean conductivity of 0.24 $\pm$ 0.08 S/cm was calculated. The measured values refer to HCl-doped CPA channels in the as-deposited, conductive emeraldine salt state, in a resistor configuration (Au-CPA-Au). The high resulting currents are on the mA scale, whereas previously typically observed on/off ratios of about 3 orders of magnitude are maintained. Interestingly, despite the large thickness of the channel, OMD switching remains possible, whereas in the case of previous devices with more compact LS-based films, lower thicknesses of 10−100 nm (corresponding to ca. 5−50 LS monolayers) are required for a sufficiently fast operation in the bottom contact/top gate configuration. This is likely due to the presence of pinholes and to the porous morphology of the AJP printed layer, both enhancing the SPE/CPA interface and hence promoting the CPA switching throughout the bulk of the material. The kinetics of the device could be improved by reducing the thickness of the layer through optimizing both the ink formulation and printing parameters, in particular the deposition stage speed. This would also lower the power consumption of the device by lowering the output current, as suggested by Van de Burgt et al.[36]

## 4. CONCLUSIONS AND OUTLOOK

Our study successfully demonstrates the realization of PANI-based solutions/suspensions well suited for preparing PANI films by automated manufacturing tools, such as 3D printing techniques for rapid prototyping, with a particular reference to the promising, industrially scalable AJP technique. Our approach has led to the determination of a fine and controlled chitosan:PANI suspension in a water/IPA-based solvent formulation, i.e., the CPA composite-based ink, which is (i) characterized by a very low polydispersity of chitosan:PANI microparticles and a very high, long-lasting stability; (ii) far more ecofriendly by avoiding solvents such as NMP usually used with pure PANI; (iii) highly suitable to AJP deposition systems in determining well-working and finely patterned films; and, importantly, (iv) capable of furnishing intrinsically conductive films, without the need for postprocessing treatments. By interfacing the as-printed CPA films with a PEO-AlCl$_3$-based SPE, we developed the first literature prototypes of a very promising, printed, CPA-based OMD with a stable memristive response (well-defined counterclockwise hysteresis and rectification). Furthermore, the devices exhibit faster switching speeds despite the resulting higher CPA film thickness, which hinders the fast response in the case of LS-coated PANI films. The present work paves the way to further improvements and developments, in particular by a finer tuning of the presented CPA ink in terms of its formulation. The properties determining the final film features such as the ink viscosity can be tuned by acting on the solvent mixing ratio and CPA particle concentration. In addition, film features such as thickness may be optimized by adjusting some deposition parameters of the AJP system, such as the stage speed and temperature.

In future works, our goal is to optimize the ink composition and printing parameters to improve the line definition and reduce overspray and porosity of the layer. This will allow us to fabricate higher performing channels for highly reproducible and reliably functioning organic memristive microdevices. Furthermore, a major goal is to advance toward a microdevice fully fabricated by direct writing techniques for rapid prototyping, including the conductive channel, source, drain, and gate electrodes, and the polyelectrolyte.

## ■ AUTHOR INFORMATION

### Corresponding Authors

**Pasquale D'Angelo** − *Institute of Materials for Electronics and Magnetism, Italian National Research Council (IMEM-CNR), 43124 Parma, Italy;* ⓘ orcid.org/0000-0002-4500-4457; Email: pasquale.dangelo@imem.cnr.it

**Salvatore Iannotta** − *Institute of Materials for Electronics and Magnetism, Italian National Research Council (IMEM-CNR), 43124 Parma, Italy;* ⓘ orcid.org/0000-0001-7743-1317; Email: salvatore.iannotta@imem.cnr.it

### Authors

**Roman Sajapin** − *Institute of Materials for Electronics and Magnetism, Italian National Research Council (IMEM-CNR), 43124 Parma, Italy; Graduate School in Science and Technologies of Materials and Department of Physics, University of Parma, 43121 Parma, Italy*

**Davide Vurro** − *Institute of Materials for Electronics and Magnetism, Italian National Research Council (IMEM-CNR), 43124 Parma, Italy; Camlin Italy S.r.l., 43123 Parma, Italy*

**Giuseppe Tarabella** − *Institute of Materials for Electronics and Magnetism, Italian National Research Council (IMEM-CNR), 43124 Parma, Italy*

**Simone L. Marasso** − *Institute of Materials for Electronics and Magnetism, Italian National Research Council (IMEM-CNR), 43124 Parma, Italy; Department of Applied Science and Technology, Politecnico di Torino, 10129 Turin, Italy*

**Matteo Cocuzza** − *Institute of Materials for Electronics and Magnetism, Italian National Research Council (IMEM-CNR), 43124 Parma, Italy; Department of Applied Science and Technology, Politecnico di Torino, 10129 Turin, Italy*

**Maddalena Botti** − *Institute of Materials for Electronics and Magnetism, Italian National Research Council (IMEM-CNR), 43124 Parma, Italy; Department of Veterinary Medical Sciences, University of Parma, 43121 Parma, Italy*

**Mirko Buttrini** − *Department of Medicine and Surgery, University of Parma, 43121 Parma, Italy*

**Adriana Calderaro** − *Department of Medicine and Surgery, University of Parma, 43121 Parma, Italy*

**Tatiana Berzina** − *Institute of Materials for Electronics and Magnetism, Italian National Research Council (IMEM-CNR), 43124 Parma, Italy*

Complete contact information is available at:
https://pubs.acs.org/10.1021/acsaelm.2c01047

### Author Contributions

R.S., P.D. T.B., and S.I. conceptualized the study; R.S., D.V., and P.D. designed the experiments; R.S., D.V., G.T., S.L.M., and M.C. prepared the OMD devices; R.S., D.V., P.D., G.T., M.Botti, M.Buttrini, and A.C. characterized the CPA

composite; R.S. and T.B. characterized the OMD response; all authors discussed the experimental results; R.S. and P.D. wrote the original manuscript, which was revised and approved in its final version by all authors; T.B. and S.I. supervised the activity.

### Notes

The authors declare no competing financial interest.

## ■ REFERENCES

(1) Xia, Q.; Yang, J. J. Memristive crossbar arrays for brain-inspired computing. *Nat. Mater.* **2019**, *18*, 309−323.

(2) Wang, W.; Pedretti, G.; Milo, V.; Carboni, R.; Calderoni, A.; Ramaswamy, N.; Spinelli, A. S.; Ielmini, D. Learning of spatiotemporal patterns in a spiking neural network with resistive switching synapses. *Sci. Adv.* **2018**, *4*, 1−9.

(3) Chua, L.O. Memristor − The missing circuit element. *IEEE Trans. Circuit Theor.* **1971**, *18*, 507−519.

(4) Kennedy, M. P.; Chua, L. O. Neural networks for nonlinear programming. *IEEE Trans. Circuit Systems* **1988**, *35*, 554−562.

(5) Ielmini, D.; Wong, H. S. P. In-memory computing with resistive switching devices. *Nat. Electron.* **2018**, *1*, 333−343.

(6) Markram, H.; Gerstner, W.; Sjöström, P. J. Spike-timing-dependent plasticity: A comprehensive overview. *Front. Synaptic Neurosci.* **2012**, *4*, 2010−2012.

(7) Li, Y.; Wang, Z.; Midya, R.; Xia, Q.; Yang, J. J. Review of memristor devices in neuromorphic computing: materials science and device challenges. *J. Phys. D Appl. Phys.* **2018**, *51*, 503002.

(8) Valov, I.; Kozicki, M. Organic memristors come of age. *Nat. Mater.* **2017**, *16*, 1170−1172.

(9) Yuan, L.; Liu, S.; Chen, W.; Fan, F.; Liu, G. Organic memory and memristors: from mechanisms, materials to devices. *Adv. Electron. Mater.* **2021**, *7*, 2100432.

(10) Erokhin, V.; Berzina, T.; Fontana, M. P. Hybrid electronic device based on polyaniline-polyethyleneoxide junction. *J. Appl. Phys.* **2005**, *97*, 064501.

(11) Cifarelli, A.; Berzina, T.; Parisini, A.; Iannotta, S. Memristive response and electrochemical processes in polyaniline based organic devices. *Org. Electron.* **2020**, *83*, 105757.

(12) Sajapin, R.; Berzina, T.; Burganova, R.; Iannotta, S. New insight in the operation mechanism of organic memristive devices: The role of PEO-based polyelectrolyte solute ions. *Org. Electron.* **2021**, *94*, 106173.

(13) Battistoni, S.; Erokhin, V.; Iannotta, S. Frequency driven organic memristive devices for neuromorphic short term and long-term plasticity. *Org. Electron.* **2019**, *65*, 434−438.

(14) Battistoni, S.; Erokhin, V.; Iannotta, S. Organic memristive devices for perceptron applications. *J. Phys. D Appl. Phys.* **2018**, *51*, 284002.

(15) Lapkin, D. A.; Emelyanov, A. V.; Demin, V. A.; Erokhin, V.; Feigin, L. A.; Kashkarov, P. K.; Kovalchuk, M. V. Polyaniline-based memristive microdevice with high switching rate and endurance. *Appl. Phys. Lett.* **2018**, *112*, 043302.

(16) Battistoni, S.; Verna, A.; Marasso, S. L.; Cocuzza, M.; Erokhin, V. On the Interpretation of Hysteresis Loop for Electronic and Ionic Currents in Organic Memristive Devices. *Phys. Status Solidi A* **2020**, *217*, 4−7.

(17) Gupta, A. A.; Bolduc, A.; Cloutier, S. G.; Izquierdo, R. Aerosol jet printing for printed electronics rapid prototyping. *IEEE ISCAS Proceedings* **2016**, 866−869.

(18) Cooper, C.; Hughes, B. Aerosol Jet Printing of electronics: An enabling technology for wearable devices. *2020 Pan Pacific Microelectronics Symposium*, **2020**.

(19) Navratil, J.; Hamacek, A.; Reboun, J.; Soukup, R. Perspective methods of creating conductive paths by Aerosol Jet Printing technology. *Int. Spring Semin. Electron. Technol. Proceedings* **2015**, 36−39.

(20) Seifert, T.; Sowade, E.; Roscher, F.; Wiemer, M.; Gessner, T.; Baumann, R. R. Additive manufacturing technologies compared: Morphology of deposits of silver ink using inkjet and aerosol jet printing. *Ind. Eng. Chem. Res.* **2015**, *54*, 769−779.

(21) Chen, G.; Gu, Y.; Tsang, H.; Hines, D. R.; Das, S. The effect of droplet sizes on overspray in Aerosol-Jet Printing. *Adv. Eng. Mater.* **2018**, *20*, 1701084.

(22) Smith, M.; Choi, Y. S.; Boughey, C.; Kar-Narayan, S. Controlling and assessing the quality of aerosol jet printed features for large area and flexible electronics. *Flex. Print. Electron.* **2017**, *2*, 015004.

(23) Tarabella, G.; Vurro, D.; Lai, S.; D'Angelo, P.; Ascari, L.; Iannotta, S. Aerosol jet printing of PEDOT:PSS for large area flexible electronics. *Flex. Print. Electron.* **2020**, *5*, 014005.

(24) Parate, K.; Rangneka, S. V.; Jing, D.; Mendivelso-Perez, D. L.; Ding, S.; Secor, E. B.; Smith, E. A.; Hostetter, J. M.; Hersam, M. C.; Claussen, J. C. Aerosol-jet-printed graphene immunosensor for label-free cytokine monitoring in serum. *ACS Appl. Mater. Interfaces* **2020**, *12*, 8592−8603.

(25) Kulkarni, M.; Viswanath, A. K. Sulphonic acids doped poly(*N*-ethyl aniline): A material for humidity sensing application. *Polym. Eng. Sci.* **2007**, *47*, 1621−1629.

(26) Bilbao, E.; Kapadia, S.; Riechert, V.; Amalvy, J.; Molinari, F. N.; Escobar, M. M.; Baumann, R. R.; Monsalve, L. N. Functional aqueous-based polyaniline inkjet inks for fully printed high-performance pH-sensitive electrodes. *Sens. Actuator B Chem.* **2021**, *346*, 130558.

(27) Ngamna, O.; Morrin, A.; Killard, A. J.; Moulton, S. E.; Smyth, M. R.; Wallace, G. G. Inkjet printable polyaniline nanoformulations. *Langmuir* **2007**, *23*, 8569−8574.

(28) Fisher, C.; Warmack, B. J.; Yu, Y.; Skolrood, L. N.; Li, K.; Joshi, P. C.; Saito, T.; Aytug, T. All-aerosol-jet-printed highly sensitive and selective polyaniline-based ammonia sensors: a route toward low-cost, low-power gas detection. *J. Mater. Sci.* **2021**, *56*, 12596−12606.

(29) Ratuchne, F.; Danczuck, M.; Guimarães de Castro, E. Enhanced Stability and Conductivity of (polyaniline/chitosan) Composites. *Orbital Electron. J. Chem.* **2018**, *10*, 239−246.

(30) Preziosi, V.; Barra, M.; Perazzo, A.; Tarabella, G.; Romeo, A.; Marasso, S. L.; D'Angelo, P.; Iannotta, S.; Cassinese, A.; Guido, S. Monitoring emulsion microstructure by using organic electrochemical transistors. *J. Mater. Chem. C* **2017**, *5*, 2056−2065.

(31) Secor, E. B. Principles of Aerosol jet Printing. *Flex. Print. Electron.* **2018**, *3*, 035002.

(32) MacDiarmid, A. G.; Chiang, J. C.; Richter, A. F.; Epstein, A. J. Polyaniline: a new concept in conducting polymers. *Synth. Met.* **1987**, *18*, 285−290.

(33) Shao, W.; Jamal, R.; Xu, F.; Ubul, A.; Abdiryim, T. The Effect of a Small Amount of Water on the Structure and Electrochemical Properties of Solid-State Synthesized Polyaniline. *Materials* **2012**, *5*, 1811−1825.

(34) Brožová, L.; Holler, P.; Kovářová, J.; Stejskal, J.; Trchová, M. The stability of polyaniline in strongly alkaline or acidic aqueous media. *Polym. Degrad. Stab.* **2008**, *93*, 592−600.

(35) Berzina, T.; Smerieri, A.; Bernab, M.; Pucci, A.; Ruggeri, G.; Erokhin, V.; Fontana, M. P. Optimization of an organic memristor as an adaptive memory element. *J. Appl. Phys.* **2009**, *105*, 124515.

(36) Van de Burgt, Y.; Melianas, A.; Keene, S. T.; Malliaras, G.; Salleo, A. Organic electronics for neuromorphic computing. *Nat. Electron.* **2018**, *1*, 386−397.